Self-Assembled Tetranuclear Square Complex of Chromium(III) Bridged by Radical Pyrazine: A Molecular Model for Metal–Organic Magnets

Dandan Lou, Nathan J Yutronkie, Itziar Oyarzabal, Long-Fei Wang, Abhijit Adak, Vincent L Nadurata, Rosa Diego, Elizaveta A Suturina, Aaron Mailman, Pierre Dechambenoit, et al.

Self-Assembled Tetranuclear Square Complex of Chromium(III) Bridged by Radical Pyrazine: A Molecular Model for Metal−Organic Magnets

Dandan Lou, Nathan J. Yutronkie, Itziar Oyarzabal, Long-Fei Wang, Abhijit Adak, Vincent L. Nadurata, Rosa Diego, Elizaveta A. Suturina, Aaron Mailman, Pierre Dechambenoit, Mathieu Rouzières, Fabrice Wilhelm, Andrei Rogalev, Sébastien Bonhommeau, Corine Mathonière, and Rodolphe Clérac*

The attractive electronic properties of metal-pyrazine materials—electrical conductivity, magnetic order, and strong magnetic coupling—can be tuned in a wide range depending on the metal employed, as well as its ligand-imposed redox environment. Using solvent-directed synthesis to control the dimensionality of such systems, a discrete tetranuclear chromium(III) complex, exhibiting a rare example of bridging radical pyrazine, has been prepared from chromium(II) triflate and neutral pyrazine. The strong antiferromagnetic interaction between Cr^{III} (S = 3/2) and radical pyrazine (S = 1/2) spins, theoretically estimated at about −932 K, leads to a thermally isolated S_T = 4 ground state, which remains the only populated state observable even at room temperature.

Coordination chemistry, a toolbox for chemists relying on the assembly of metal ions and ligands in a programmed fashion, has evolved into a powerful strategy for achieving molecule-based materials that display tailored physical properties,[1,2] useful for many applications.[3−5] In the context of metal−organic systems displaying high-temperature magnetic order and/or high electrical conductivity, the judicious choice of each structural unit is essential to achieve the necessary long-range alignment of magnetic spins, as well as the electron delocalization through the system.

The use of diamagnetic organic ligands to bridge paramagnetic metal ions often results in weak magnetic coupling and localized electronic structures. Alternatively, radical ligands can lead to high delocalization and facilitate strong magnetic interactions owing to their partially filled orbitals. Hence, the metal-radical approach has been extensively used in the field of molecular magnetism,[6] where organic radicals are typically isolated before their subsequent assembly with metal ion centers.[7,8] Frequently, radical ligands have also been introduced through post-synthetic redox treatment of complexes and materials containing closed-shell ligands.[9−12] An alternative, however, to save time, reactants, and reduce chemical waste, is to explore the possibility of *in-situ* redox processes between the metal ion and the ligand during the synthesis. By rationally selecting the metal/ligand pair based on their respective redox properties, both energies and overlaps of magnetically relevant molecular orbitals (MOs) can be tuned to attain the desired magnetic and transport properties.[13−15] Through this approach, molecule-based magnets with critical temperatures above room temperature have been obtained from the tetracyanoethylene (TCNE) radical and its analogues.[16−18]

Among other redox-active ligands, pyrazine (pyz), a ditopic aromatic ligand, is an excellent choice due to its low-lying MOs and ability to direct linear coordination geometries. While a plethora of metal−organic structures have been reported with neutral pyrazine,[19−21] it is only in the past few years that its redox non-innocence has been exploited. For instance, the redox synergy between samarium and pyrazine has been reported to lead to valence tautomerism and thermal bistability in a one-dimensional coordination polymer.[22] Meanwhile, an exceptional coercivity of 6.5 T was observed at 1.8 K in a tetranuclear dysprosium single-molecule magnet with bridging radical pyrazines.[8] Recently, our team has focused on understanding the electronic synergy between pyrazine and early 3*d* transition metals.[13−15] The redox reaction between pyrazine and Ti^{II} or Cr^{II} salts gives rise to conductive coordination solids, $Ti^{III}Cl_2[(pyz)_2^{\bullet-}]$ or $Cr^{III}Cl_2[(pyz)_2^{\bullet-}]$, respectively. In these materials, an *in-situ* metal-to-ligand charge transfer, concomitant to the self-assembly, generates a square two-dimensional (2D) coordination network with Ti^{III}/Cr^{III} metal ions and formally one reduced pyrazine ligand per formula unit. In contrast, the *in-situ* reduction is absent for the vanadium analogue $V^{II}Cl_2(pyz)_2$, as is the case for the late 3*d* metal ion analogues.[19−21] The resulting magnetic and conductive performance can thus be tuned in a wide range leading to (i) a paramagnetic, strongly correlated metal (M =

Ti), (ii) a ferrimagnetic semiconductor (M = Cr), or (iii) an antiferromagnetic insulator (M = V).[13,14] The electronic structure of the 2D $ML_2(pyz)_2$ networks is also influenced via the axially coordinated ligand (L), as exemplified in the antiferromagnetic insulator $Cr^{II}(OSO_2CH_3)_2(pyz)_2$ (L = OSO_2CH_3), for which the metal-to-pyrazine charge transfer is disabled.[15]

The aforementioned $MCl_2(pyz)_2$ compounds were synthesized exclusively in solvothermal conditions, leading to crystalline materials but not to ones suitable for single-crystal X-ray diffraction (SCXRD).[12,13] Therefore, our group has investigated solution-based methods to improve the crystallinity of these systems. The use of coordinating solvents to compete with pyrazine in the first coordination sphere of the metal ions also opens up the possibility of controlling the dimensionality of these systems, which could drastically modify their physical properties.

Taking all of this into account, we have investigated the reaction of chromium(II) ions with pyrazine in *N*,*N*-dimethylacetamide (DMA). Vapor diffusion of diethyl ether (Et_2O) into a DMA solution of chromium(II) triflate and a large excess of pyrazine afforded single crystals of **1** (Scheme 1, see Supporting Information), which crystallizes in the triclinic $P\bar{1}$ space group. As evidenced by SCXRD data collected at 120 K (Figure 1, Table S1, Figures S1 and S2), the asymmetric unit of **1** consists of four crystallographically unique Cr ions and bridging pyrazine ligands forming the vertices and the sides of a tetranuclear square complex. The Cr metal ions adopt an octahedral coordination geometry with two *cis*-arranged pyrazine ligands and the four remaining coordination sites occupied by oxygen atoms from DMA moieties, restricting the dimensionality to a zero-dimensional discrete complex. The four pyrazine rings in the square molecule are inclined by dihedral angles of 38.815(1)−40.361(2)° with respect to the mean plane intersecting the four Cr ions (Figure S2, Table S2). Eight triflate anions surround the tetranuclear complex, together with uncoordinated lattice-solvent molecules. Due to their highly disordered arrangement, however, only one DMA and one pyrazine could be resolved clearly within the void space. To determine the remaining identity and number of the guest molecules, combined outputs of thermogravimetric analysis (TGA) (Figure S3), elemental analysis (EA), and the SQUEEZE function of PLATON[23] were used to give the following chemical formula for **1**: $[Cr_4(pyz)_4(DMA)_{16}](OTf)_8{\cdot}(pyz)(DMA)_{6.7}$. Structural metrics from the SCXRD data provided initial evidence for an intramolecular redox reaction between chromium and pyrazine (Table S2). The Cr−N bond lengths at 120 K, d_{Cr-N} = 1.964(4)−1.986(5) Å, are significantly shorter than the d_{Cr-N} value of 2.149(4) Å in the Cr^{II} system $Cr^{II}I_2(pyz)_2$,[24] and are much closer to, and even shorter than, the Cr−N bond lengths in the Cr^{III} analogues $Cr^{III}Cl_2[(pyz)_2^{\bullet-}]$ and $Cr^{III}Br_2[(pyz)_2^{\bullet-}]$ (d_{Cr-N} = 2.018(3)−2.081(4) Å), strongly supporting a +3 oxidation state of chromium in **1** (Table S3).[13,24] Moreover, bond valence sum (BVS) calculations[25] (Table S4) of the Cr ions in **1** also support a +3 metal oxidation state.

Further insight into the oxidation state of the Cr ion in **1** was provided by X-ray absorption spectroscopy. X-ray absorption near-edge structure (XANES) spectra (Figure 2) were collected at the Cr K-edge for **1** and a model complex, $Cr^{III}Cl_2[(pyz)_2^{\bullet-}]$, which possesses Cr sites in an octahedral coordination geometry and an established +3 oxidation state.[13] The weak pre-edge feature, involving 1*s* to 3*d* quadrupolar transitions, is directly sensitive to the occupation of the 3*d* orbitals and thus is considered as a fingerprint of the transition metal oxidation state. As shown in Figure 2 (inset), the energy of the pre-edge transitions of **1** clearly coincides with those of the octahedral Cr^{III} reference, unambiguously confirming the same oxidation state of Cr in **1** and $Cr^{III}Cl_2[(pyz)_2^{\bullet-}]$. The difference between the XANES spectra can be attributed to the difference in the Cr coordination sphere ($\{CrO_4N_2\}$ versus $\{CrN_4Cl_2\}$) and also in dimensionality between the molecular complex **1** and the 2D reference compound $Cr^{III}Cl_2[(pyz)_2^{\bullet-}]$.

Scheme 1. Synthetic Route to 1[a]

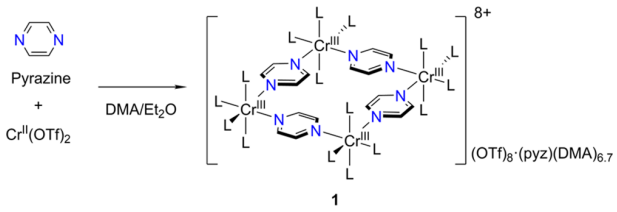

[a]L = *N*,*N*-dimethylacetamide (DMA); $^-$OTf = $^-OSO_2CF_3$ = triflate anion.

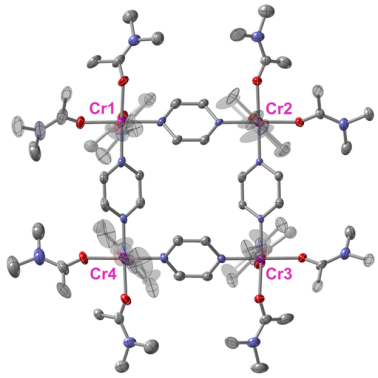

Figure 1. View of the cationic complex $[Cr_4(pyz)_4(DMA)_{16}]^{8+}$ in **1** from its X-ray crystal structure at 120 K with thermal ellipsoids drawn at the 50% probability level. Hydrogen atoms, uncoordinated pyrazine, solvent molecules (DMA), and triflate anions are omitted for clarity. The coordinated DMA molecules above and behind the $\{Cr_4(pyz)_4\}$ plane are shown in 60% transparency for clarity. Color code: light blue, N; light gray, C; red, O; pink, Cr.

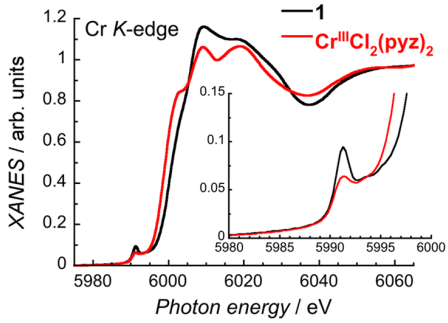

Figure 2. Normalized XANES spectra at the Cr K-edge for **1** (black trace) and the Cr^{III} reference compound, $Cr^{III}Cl_2[(pyz)_2^{\bullet-}]$, (red trace) at 295 K. Inset: magnified view of the pre-edge region.

In the 2D system, a higher degree of hybridization with the surrounding ligands results in higher intensity of the shoulder at the rising edge (ca. 6000 eV).[13]

The presence of eight triflate anions in the crystal structure implies a +8 charged tetranuclear Cr^{III} unit, which suggests that the four bridging pyrazines are singly reduced within the molecule so as to balance the charge. Looking at the structural parameters of the pyrazine ligands in **1**, the average C−N bond length (d_{C-N} = 1.370 Å) is longer than the average C−C bond length (d_{C-C} = 1.359 Å) (Table S2). Such structural characteristics support the presence of singly reduced pyrazines, based on (i) comparison with other systems containing pyrazine in radical or neutral forms,[12−15] as well as (ii) gas-phase bond distances for neutral pyrazine and its radical-anion determined from density functional theory (DFT) calculations.[12] In addition, Raman measurements are also consistent with the presence of reduced pyrazine bridges (Figure S4) based on the energy of the **8a** vibrational mode, which involves symmetrical C═C stretching and C−H scissoring.[12]

The magnetic properties of **1** were studied by dc susceptibility (χ) measurements shown as a χT vs T plot in Figure 3 (see Supporting Information). A quasi-constant χT

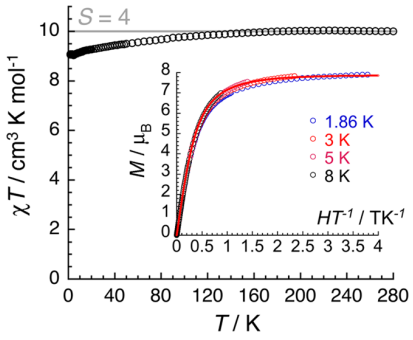

Figure 3. Temperature (T) dependence of the χT product at 0.1 T for **1** (where $\chi = M/H$ is the molar magnetic susceptibility normalized per complex). Inset: Field (H) dependence of the magnetization (M) for **1** below 8 K plotted as M vs HT^{-1}. The solid red line is the best fit of the experimental data to the S_T = 4 Brillouin function.

product of around 10.0 cm^3 K mol^{-1} above 160 K and then a gradual decrease down to 9.1 cm^3 K mol^{-1} at 1.85 K demonstrate paramagnetic behavior in the whole temperature range. These values are compatible with two limiting cases: (i) magnetically isolated or (ii) strongly antiferromagnetically coupled spins, the latter of which is expected, from comparison with related systems.[13,26] In the first hypothesis, the theoretical χT value of 9 cm^3 K mol^{-1} (g = 2) is derived by the simple sum of the Curie constants for uncoupled spins from four Cr^{III} and four $pyz^{\bullet-}$ radical centers. In the second case, 10 cm^3 K mol^{-1} (g = 2) is expected for an S_T = 4 ground spin state, resulting from four S = 3/2 Cr^{III} spins antiferromagnetically coupled to four S = 1/2 $pyz^{\bullet-}$ radicals. The field dependence of the magnetization at low temperatures helps to discriminate between these two hypotheses. The magnetization of **1** at 1.86 K reaches 7.9 μ_B under 7 T (Figure 3, inset), pointing toward case (ii), for which the proposed S_T = 4 ground state has an expected saturation value of 8 μ_B. Accordingly, the M vs HT^{-1} data can be fitted relatively well to a simple S = 4 Brillouin function below 8 K, yielding g = 1.95(5).

To estimate the strength of the magnetic coupling between Cr^{III} and $pyz^{\bullet-}$ spins in **1**, DFT calculations were performed based on the single-crystal structural metrics. The computed spin-density distributions of the high-spin state (S_T = 8) and the broken-symmetry solution (S_T = 4) where pyrazine radical spins are flipped are illustrated in Figure 4. The Mulliken spin

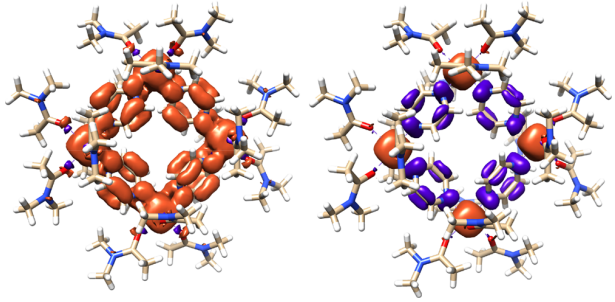

Figure 4. View of the computed spin density of the high-spin state (left) and the broken-symmetry solution (right) for **1**. The bright coral and purple colors indicate the spin-up and spin-down densities. The contour value for the plot is 0.003.

population suggests that the complete reduction of all pyrazines has taken place, creating a $[Cr^{III}_4(pyz^{\bullet-})_4]^{8+}$ system, as supported by the physical characterization (*vide supra*). The calculated broken-symmetry S_T = 4 state (B3LYP/def2-TZVP level of theory) is lower in energy, confirming the presence of an antiferromagnetic exchange coupling between neighboring spins of the metal ions and the pyrazine radical sites. Using an Ising spin Hamiltonian, the estimated exchange coupling constant is −648 cm^{-1} (−932 K; Table S5). Notably, this value is about three times smaller than the predicted value between Cr^{III} and partially reduced pyrazine spins in the 2D network, $Cr^{III}Cl_2[(pyz)_2^{\bullet-}]$ (−1912 cm^{-1}).[13] However, the antiferromagnetic coupling is strong enough in **1** to thermally populate only the ground S_T = 4 state at room temperature, as inferred from the flatness of the χT vs T data (Figure 3).

In summary, the redox reaction of $Cr^{II}(OTf)_2$ and pyrazine in *N*,*N*-dimethylacetamide favors the formation of a discrete tetranuclear square $[Cr^{III}_4(pyz^{\bullet-})_4]^{8+}$ complex, demonstrating the role that solvent plays in influencing the dimensionality and redox properties of metal-pyrazine compounds. In comparison to previously reported molecular square systems,[27−32] this complex is a rare example of a molecular unit bearing pyrazine radical ligands. This strongly correlated square system should serve as a molecular model for the ever-expanding family of metal-pyrazine coordination networks, its detailed characterization representing a comprehensive resource toward a deeper understanding of its extended analogs. Furthermore, the synthesis of a chromium-pyrazine system via solution-based techniques can easily be extended to other metal ions, endowing **1** with the potential to serve as a building block for the formation of high-performance crystalline molecule-based magnetic materials.

Corresponding Author

Rodolphe Clérac − *Univ. Bordeaux, CNRS, CRPP, UMR 5031, F-33600 Pessac, France;* orcid.org/0000-0001-5429-7418; Email: rodolphe.clerac@u-bordeaux.fr

Authors

Dandan Lou − *Univ. Bordeaux, CNRS, CRPP, UMR 5031, F-33600 Pessac, France*

Nathan J. Yutronkie − *Univ. Bordeaux, CNRS, CRPP, UMR 5031, F-33600 Pessac, France*

Itziar Oyarzabal − *BCMaterials, Basque Center for Materials, Applications and Nanostructures, ES-48940 Leioa, Spain; IKERBASQUE, Basque Foundation for Science, ES-48009 Bilbao, Spain;* orcid.org/0000-0001-9149-2511

Long-Fei Wang − *Univ. Bordeaux, CNRS, CRPP, UMR 5031, F-33600 Pessac, France*

Abhijit Adak − *Univ. Bordeaux, CNRS, CRPP, UMR 5031, F-33600 Pessac, France*

Vincent L. Nadurata − *Univ. Bordeaux, CNRS, CRPP, UMR 5031, F-33600 Pessac, France;* orcid.org/0000-0003-2991-7851

Rosa Diego − *Univ. Bordeaux, CNRS, CRPP, UMR 5031, F-33600 Pessac, France;* orcid.org/0000-0003-1158-522X

Elizaveta A. Suturina − *Department of Chemistry, University of Bath, Bath BA2 7AY, U.K.;* orcid.org/0000-0003-4407-1882

Aaron Mailman − *Department of Chemistry, NanoScience Centre, University of Jyväskylä, FI-40014 Jyväskylä, Finland;* orcid.org/0000-0003-2067-8479

Pierre Dechambenoit − *Univ. Bordeaux, CNRS, CRPP, UMR 5031, F-33600 Pessac, France;* orcid.org/0000-0001-7850-2260

Mathieu Rouzières − *Univ. Bordeaux, CNRS, CRPP, UMR 5031, F-33600 Pessac, France*

Fabrice Wilhelm − *ESRF − The European Synchrotron, CS 40220, F-38043 Grenoble Cedex 9, France*

Andrei Rogalev − *ESRF − The European Synchrotron, CS 40220, F-38043 Grenoble Cedex 9, France*

Sébastien Bonhommeau − *Univ. Bordeaux, CNRS, Bordeaux INP, ISM, UMR 5255, F-33400 Talence, France;* orcid.org/0000-0002-9213-7201

Corine Mathonière − *Univ. Bordeaux, CNRS, CRPP, UMR 5031, F-33600 Pessac, France;* orcid.org/0000-0002-4774-1610

This work was supported by the University of Bordeaux, the Région Nouvelle Aquitaine, Quantum Matter Bordeaux, the ANR (HiPerMagnet project, ANR-20-CE07-0022), the Centre National de la Recherche Scientifique (CNRS), the European Synchrotron (ESRF), and the China Scholarship Council (CSC) for the Ph.D. funding of D.L. I.O. acknowledges financial support from the Department of Education of the Basque Government through the PIBA project call (PIBA_2023_1_0027). S.B. thanks the platform SIV (Spectroscopie et Imagerie Vibrationnelle) funded by the European Union (FEDER) and the Région Nouvelle Aquitaine. A.M. acknowledges financial support from the Academy of Finland (Project 336456).

(1) Batten, S. R.; Neville, S. M.; Turner, D. R. *Coordination Polymers: Design, Analysis and Applications*, 1st ed.; RSC Publishing, 2009.

(2) Coronado, E. Molecular magnetism: from chemical design to spin control in molecules, materials and devices. *Nat. Rev. Mater.* **2020**, *5*, 87−104.

(3) Sumida, K.; Rogow, D. L.; Mason, J. A.; McDonald, T. M.; Bloch, E. D.; Herm, Z. R.; Bae, T. H.; Long, J. R. Carbon dioxide capture in metal−organic frameworks. *Chem. Rev.* **2012**, *112*, 724−781.

(4) Bloch, E. D.; Queen, W. L.; Krishna, R.; Zadrozny, J. M.; Brown, C. M.; Long, J. R. Hydrocarbon separations in a metal-organic framework with open iron(II) coordination sites. *Science* **2012**, *335*, 1606−1610.

(5) Wu, M.-X.; Yang, Y.-W. A fluorescent pillarene coordination polymer. *Polym. Chem.* **2019**, *29*, 2980−2985.

(6) Caneschi, A.; Gatteschi, D.; Sessoli, R.; Rey, P. Toward molecular magnets: the metal-radical approach. *Acc. Chem. Res.* **1989**, *22*, 392−398.

(7) Benner, F.; Demir, S. From unprecedented 2,2′-bisimidazole-bridged rare earth organometallics to magnetic hysteresis in the dysprosium congener. *Inorg. Chem. Front.* **2023**, *10*, 4981−4992.

(8) Bajaj, N.; Mavragani, N.; Kitos, A. A.; Chartrand, D.; Maris, T.; Mansikkamäki, A.; Murugesu, M. Hard Single-Molecule Magnet Behavior and Strong Magnetic Coupling in Radical-Bridged Ln_2 and Ln_4 Metallocenes. *Chem.*, 2024, in press DOI: 10.1016/j.chempr.2024.04.006.

(9) Impert, O.; Witwicki, M.; Komarnicka, U. K.; Bieńko, A.; Niorettini, A.; Chatterjee, D. Redox reactions of a pyrazine-bridged Ru^{III}(edta) binuclear complex: spectrochemical, spectroelectrochemical and theoretical studies. *Phys. Chem. Chem. Phys.* **2024**, *26*, 3981−3989.

(10) Liu, L.; Degayner, J. A.; Sun, L.; Zee, D. Z.; Harris, T. D. Reversible redox switching of magnetic order and electrical conductivity in a 2D manganese benzoquinoid framework. *Chem. Sci.* **2019**, *10*, 4652−4661.

(11) Ma, X.; Suturina, E. A.; De, S.; Négrier, P.; Rouzières, M.; Clérac, R.; Dechambenoit, P. A Redox-Active Bridging Ligand to Promote Spin Delocalization, High-Spin Complexes, and Magnetic Multi-Switchability. *Angew. Chem., Int. Ed.* **2018**, *57*, 7841−7845.

(12) Perlepe, P.; Oyarzabal, I.; Mailman, A.; Yquel, M.; Platunov, M.; Dovgaliuk, I.; Rouzières, M.; Négrier, P.; Mondieig, D.; Suturina, E. A.; Dourges, M. A.; Bonhommeau, S.; Musgrave, R. A.; Pedersen, K. S.; Chernyshov, D.; Wilhelm, F.; Rogalev, A.; Mathonière, C.; Clérac, R. Metal-organic magnets with large coercivity and ordering temperatures up to 242°C. *Science* **2020**, *370*, 587−592.

(13) Pedersen, K. S.; Perlepe, P.; Aubrey, M. L.; Woodruff, D. N.; Reyes-Lillo, S. E.; Reinholdt, A.; Voigt, L.; Li, Z.; Borup, K.; Rouzières, M.; Samohvalov, D.; Wilhelm, F.; Rogalev, A.; Neaton, J. B.; Long, J. R.; Clérac, R. Formation of the layered conductive magnet $CrCl_2$(pyrazine)$_2$ through redox-active coordination chemistry. *Nat. Chem.* **2018**, *10*, 1056−1061.

(14) Perlepe, P.; Oyarzabal, I.; Voigt, L.; Kubus, M.; Woodruff, D. N.; Reyes-Lillo, S. E.; Aubrey, M. L.; Négrier, P.; Rouzières, M.; Wilhelm, F.; Rogalev, A.; Neaton, J. B.; Long, J. R.; Mathonière, C.; Vignolle, B.; Pedersen, K. S.; Clérac, R. From an antiferromagnetic insulator to a strongly correlated metal in square-lattice $MCl_2(pyrazine)_2$ coordination solids. *Nat. Commun.* **2022**, *13*, 5766.
(15) Perlepe, P.; Oyarzabal, I.; Pedersen, K. S.; Negrier, P.; Mondieig, D.; Rouzières, M.; Hillard, E. A.; Wilhelm, F.; Rogalev, A.; Suturina, E. A.; Mathonière, C.; Clérac, R. $Cr(pyrazine)_2(OSO_2CH_3)_2$: a two-dimensional coordination polymer with an antiferromagnetic ground state. *Polyhedron* **2018**, *153*, 248−253.
(16) Miller, J. S.; Ohkoshi, S. *Molecular Magnetic Materials: Concepts and Applications*; Wiley-VCH, 2017.
(17) Manriquez, J. M.; Yee, G. T.; Mclean, R. S.; Epstein, A. J.; Miller, J. S. A Room-Temperature Molecular/Organic-Based Magnet. *Science* **1991**, *252*, 1415−1417.
(18) Pokhodnya, K. I.; Epstein, A. J.; Miller, J. S. Thin-Film V[TCNE]x Magnets. *Adv. Mater.* **2000**, *12*, 410−413.
(19) Haynes, J. S.; Sams, J. R.; Thompson, R. C. Magnetic and Spectroscopic Study of Pyrazine-Bridged Iron (II) Halide Complexes. *Inorg. Chem.* **1986**, *25*, 3740−3744.
(20) De Campos, E. A.; Silva, N. J. O.; Shi, F. N.; Rocha, J. Cobalt(II)-pyrazine-chloride coordination polymers: Synthesis, reactivity and magnetic properties. *CrystEngComm* **2014**, *16*, 10439−10444.
(21) Liu, J.; Goddard, P. A.; Singleton, J.; Brambleby, J.; Foronda, F.; Möller, J. S.; Kohama, Y.; Ghannadzadeh, S.; Ardavan, A.; Blundell, S. J.; Lancaster, T.; Xiao, F.; Williams, R. C.; Pratt, F. L.; Baker, P. J.; Wierschem, K.; Lapidus, S. H.; Stone, K. H.; Stephens, P. W.; Bendix, J.; Woods, T. J.; Carreiro, K. E.; Tran, H. E.; Villam, C. J.; Manson, J. L. Antiferromagnetism in a Family of S = 1 Square Lattice Coordination Polymers $NiX_2(pyz)_2$ (X = Cl, Br, I, NCS; Pyz = Pyrazine). *Inorg. Chem.* **2016**, *55*, 3515−3529.
(22) Dunstan, M. A.; Manvell, A. S.; Yutronkie, N. J.; Aribot, F.; Bendix, J.; Rogalev, A.; Pedersen, K. S. Tunable valence tautomerism in lanthanide−organic alloys. *Nat. Chem.* **2024**, *16*, 735−740.
(23) Spek, A. L. PLATON SQUEEZE: a tool for the calculation of the disordered solvent contribution to the calculated structure factors. *Acta Crystallogr. Sect. C Struct. Chem.* **2015**, *71*, 9−18.
(24) Voigt, L. *Radical Architectures in Two Dimensions*; Technical University of Denmark, 2020.
(25) Brown, I. D.; Altermatt, D. Bond-valence parameters obtained from a systematic analysis of the inorganic crystal structure database. *Acta Crystallogr. Sect. B* **1985**, *41*, 244−247.
(26) Ma, X.; Suturina, E. A.; Rouzières, M.; Wilhelm, F.; Rogalev, A.; Clérac, R.; Dechambenoit, P. A heteroleptic diradical Cr(III) complex with extended spin delocalization and large intramolecular magnetic exchange. *Chem. Commun.* **2020**, *56*, 4906−4909.
(27) Slone, R. V.; Hupp, J. T.; Stern, C. L.; Albrecht-Schmitt, T. E. Self-assembly of luminescent molecular squares featuring octahedral rhenium corners. *Inorg. Chem.* **1996**, *35*, 4096−4097.
(28) Karthikeyan, S.; Velavan, K.; Sathishkumar, R.; Varghese, B.; Manimaran, B. Self-assembly of manganese(I)-based molecular squares: Synthesis and spectroscopic and structural characterization. *Organometallics* **2012**, *31*, 1953−1957.
(29) Willermann, M.; Mulcahy, C.; Sigel, R. K. O.; Cerdà, M. M.; Freisinger, E.; Sanz Miguel, P. J.; Roitzsch, M.; Lippert, B. Pyrazine as a Building Block for Molecular Architectures with Pt^{II}. *Inorg. Chem.* **2006**, *45*, 2093−2099.
(30) Kraft, S.; Hanuschek, E.; Beckhaus, R.; Haase, D.; Saak, W. Titanium-Based Molecular Squares and Rectangles: Syntheses by Self-Assembly Reactions of Titanocene Fragments and Aromatic N-Heterocycles. *Chem.—Eur. J.* **2005**, *11*, 969−978.
(31) Kraft, S.; Beckhaus, R.; Haase, D.; Saak, W. Directed Reduction of Six-Membered Nitrogen Heterocycles—Selective Formation of Polynuclear Titanium Complexes. *Angew. Chem., Int. Ed.* **2004**, *43*, 1583−1587.
(32) Lau, V. C.; Berben, L. A.; Long, J. R. $[(Cyclen)_4Ru_4(pz)_4]^{9+}$: A Creutz−Taube Square. *J. Am. Chem. Soc.* **2002**, *124*, 9042−9043.

Supporting Information for

Self-assembled tetranuclear square complex of chromium(III) bridged by radical pyrazine: a molecular model for metal-organic magnets

Dandan Lou,[a] Nathan J. Yutronkie,[a] Itziar Oyarzabal,[b,c] Long-Fei Wang,[a] Abhijit Adak,[a] Vincent L. Nadurata,[a] Rosa Diego,[a] Elizaveta A. Suturina,[d] Aaron Mailman,[e] Pierre Dechambenoit,[a] Mathieu Rouzières,[a] Fabrice Wilhelm,[f] Andrei Rogalev,[f] Sébastien Bonhommeau,[g] Corine Mathonière[a] and Rodolphe Clérac[a]*

Email: rodolphe.clerac@u-bordeaux.fr

[a] Univ. Bordeaux, CNRS, CRPP, UMR 5031, F-33600 Pessac, France.
[b] BCMaterials, Basque Center for Materials, Applications and Nanostructures, UPV/EHU Science Park, ES-48940 Leioa, Spain.
[c] IKERBASQUE, Basque Foundation for Science, ES-48009 Bilbao, Spain.
[d] Department of Chemistry, University of Bath, Claverton Down, Bath BA2 7AY, UK.
[e] University of Jyväskylä, Department of Chemistry, NanoScience Centre, P.O. Box 35, FI-40014 Jyväskylä, Finland.
[f] ESRF — The European Synchrotron, CS 40220, F-38043 Grenoble Cedex 9, France.
[g] Univ. Bordeaux, CNRS, Bordeaux INP, ISM, UMR 5255, F-33400 Talence, France.

Table of Contents

Materials and methods

General information. All chemicals (anhydrous DMA, pyrazine, trifluoromethanesulfonic acid and chromium powder) were of reagent grade and used as received, unless otherwise noted. Chromium triflate, $Cr(OTf)_2$, was synthesized analogously to the previously described synthesis of chromium methanesulfonate, $Cr(OSO_2CH_3)_2$, with triflic acid instead of methanesulfonic acid, as described below.[1] Diethyl ether (Et_2O) was dried by passing through activated alumina on an Innovative Technology solvent-purification system and subsequently stored over 4 Å molecular sieves. All manipulations were performed by standard Schlenk techniques and/or in a glovebox under an inert and controlled dinitrogen or argon atmosphere, due to the air-sensitivity of some of the reagents and final products.

Preparation of anhydrous $Cr(OTf)_2$. A suspension of chromium powder (4.0 g, 77 mmol) and triflic acid (10 mL, 115 mmol) in 20 mL of degassed water was refluxed overnight. The dark blue suspension was filtered under argon while still hot to remove the unreacted Cr powder. The solvent was then removed under reduced pressure, and the pale grey powder was dried under dynamic vacuum at 200°C for 12 hours. Yield: 12.1 g, 60%. IR ($\bar{\nu}_{max}$, ATR): 1362 (w), 1260 (m), 1211 (s), 1193 (s), 1035 (s), 733 (w), 628 (s), 593 (s), 584 (m), 524 (s) cm^{-1}.

Preparation of $[Cr_4(pyz)_4(DMA)_{16}](OTf)_8(pyz)(DMA)_{6.7}$ (1). 75 mg of $Cr(OTf)_2$ (0.21 mmol, 1 eq.) and 255 mg of pyrazine (3.19 mmol, 15 eq.) were dissolved into 1 mL of DMA in a 6 mL glass vial. The open vial was placed into a 20 mL glass vial containing 6 mL Et_2O. The outer vial was sealed and Et_2O was allowed to diffuse into the inner vial, resulting in a precipitate appearing after 3 days. The resulting solid was collected by filtration on a Whatman™ Grade 2V filter paper (porosity size > 8 µm), washed with 3 mL of Et_2O and dried in the glovebox atmosphere. Deep blue, block-shape crystals, suitable for single-crystal X-ray diffraction were selected from the bulk solid. Isolated yield: 350 mg, 44% based on $Cr(OTf)_2$. IR ($\bar{\nu}_{max}$, ATR): 3120 (w), 2950 (w), 1595 (vs), 1500 (s), 1425 (s), 1405 (s), 1365 (w), 1255 (vs), 1223 (m), 1200 (w), 1146 (s), 1076 (m), 1060 (w), 1030 (vs), 1020 (vs), 970 (m), 805 (m), 752 (s), 633 (vs), 596 (m), 570 (m), 516 (m), 493 (m), 446 (m), 416 (m) cm^{-1}. Elemental analysis for $C_{110.8}H_{206.3}Cr_4F_{24}N_{30.7}O_{44.7}S_8$, $[Cr_4(pyz)_4(DMA)_{16}](OTf)_8 \cdot (pyz)(DMA)_{4.7}$ calculated: C, 36.92; H, 5.77; N, 11.93 %; Found: C, 36.66; H, 5.36; N: 12.18 %. **Note**: The amount of uncoordinated DMA solvent molecules (4.7) obtained from elemental analysis measurements is lower than the expected value from single-crystal X-ray diffraction measurements (6.7). This difference arises from the easy loss of DMA from the structure during manipulations (see Figure S3), which is a common

phenomenon when a material contains a large amount of interstitial lattice solvent molecules (6.7 DMA molecules and 1 uncoordinated pyrazine per 4 Cr centers; see Figure S1).

Infrared spectroscopy. The measurements were perfomed on solid samples at room temperature using an Agilent Technologies Cary 630 FT-IR spectrometer in a glovebox under an inert dinitrogen atmosphere.

Elemental analysis. The results were obtained using a Vario EL III element analyzer at the Department of Chemistry of the University of Jyväskylä, Finland. The errors on the C, H and N values are estimated between 0.5% and 0.1% (0.1% corresponds to the error in the ideal standard conditions given by the Vario element analyser).

Crystallographic methods and results. The single-crystal diffraction experiments were performed on a Bruker APEX II Quasar diffractometer using graphite monochromated MoKα radiation (λ = 0.71073 Å). Single crystals for analysis were mounted on fiber CryoLoops coated with Cargille^{TM} NHV immersion oil and cooled down to 120 K prior to data collection. The collected data were integrated and thereafter corrected for absorption with the programs SAINT and SADABS,[2] respectively. The structures were solved using direct methods and refined with the SHELXL-2018 refinement package with full-matrix least-squares procedures based on F^2.[3] All non-hydrogen atoms were refined with anisotropic displacement parameters. Hydrogen atoms were assigned to ideal positions and refined isotropically using a riding model using isotropic displacement parameters corresponding to 1.2 (aromatic) and 1.5 (aliphatic) times the host atom. Notably, the crystal structure contains at least one uncoordinated pyrazine molecule, and several interstitial DMA molecules. One of these DMA molecules was well defined, but it was impossible to model the rest of the DMA molecules properly without using an inappropriate number of constraints. Hence, these latter DMA molecules associated with highly disordered arrangements were treated as a diffuse contribution to the overall scattering without specific atom positions using the SQUEEZE procedure in PLATON.[4] Based on the electronic density, and the resultant void space volume calculated by PLATON, and assuming that only DMA molecules are present, the compound contains 5 or 6 additional uncoordinated molecules of DMA per macrocycle (calculated value: 5.7 according to the electronic density). Thus, the formula of this compound was determined as $[Cr_4(pyz)_4(DMA)_{16}](OTf)_8(pyz)(DMA)_{6.7}$ with a chemical formula of $C_{118.8}H_{224.3}Cr_4F_{24}N_{32.7}O_{46.7}S_8$ and molecular weight of 3778.61 g.mol^{-1}. Figures S1 and S2 related to the crystal structures were generated using Diamond® by Crystal Impact GbR, Bonn, Germany (https://www.crystalimpact.com/). Figure 1 was generated using

CrystalMaker®: a crystal and molecular structures program for Mac and Windows. CrystalMaker Software Ltd, Oxford, England (www.crystalmaker.com).

Thermogravimetric analysis (TGA). The measurement was carried out under a dinitrogen flow of 25 mL min^{-1} at a rate of 2 K min^{-1} on a TA Q50 thermobalance. The freshly prepared and extremely air-sensitive sample was pre-weighed on a microanalytical balance inside a glovebox and protected with a layer of (frozen) cyclohexane in the pan under a dinitrogen atmosphere prior to introduction to the sample chamber of the TGA. The cyclohexane was allowed to evaporate under the resultant dinitrogen atmosphere.

Raman spectroscopy. A commercial (XploRA, Horiba scientific) confocal Raman spectrometer, which is equipped with a motorized *xy* stage, a 1200 grooves mm^{-1} grating, and a long working distance ×50 Olympus objective with 0.45 numerical aperture, was used for the Raman scattering experiments. The samples were sealed into quartz capillaries of 0.7 mm diameter with wax and irradiated at 785 nm with a 0.37 mW laser power.

X-ray absorption spectroscopy (XAS). X-ray absorption experiments were performed at the ID12 beamline of the European Synchrotron Radiation Facility (ESRF). The X-ray source for the Cr K-edge experiments was the second harmonic of a Helios-II type undulator (HU-52). To minimize radiation damage, a 50-μm thick Al attenuator was inserted upstream of a double crystal Si <111> monochromator. Pressed powders of the crystalline solids were mounted inside an argon filled glovebox into vacuum tight sample holders covered with 13-μm thick Kapton foil.

Magnetic susceptibility measurements. The magnetic measurements were carried out with a Quantum Design MPMS-XL SQUID magnetometer and a PPMS-9 susceptometer. The MPMS-XL instrument works between 1.85 and 400 K with applied static fields (H) ranging from –7 to 7 T. The data were collected on fresh-filtered crystalline samples (≈ 10 mg; seven different batches were measured to ensure the reproducibility of the reported results). The samples were first sealed in an argon-filled glovebox in a polypropylene bag (size ≈ 1 × 0.5 × 0.02 cm) and subsequently in an additional polypropylene bag (size ≈ 2 × 1 × 0.02 cm) to ensure a complete protection from oxygen and humidity. The resulting data were corrected for the sample holder and intrinsic diamagnetic contributions of the sample. The alternating current (*ac*) susceptibility measurements down to 1.9 K were performed using an oscillating field of 1–6 Oe for frequencies (ν) from 1 to 10 kHz and applied static fields of zero to 10 kOe (PPMS-9). In the available temperature (>1.85 K) and frequency ranges (1 Hz–10 kHz), the sample does not display any slow relaxation of the magnetization observable in zero and in finite applied *dc* fields.

Regarding the gradual decrease of the χT value below 150 K (Figure 3), the origin of this thermal behavior is unlikely to be weak antiferromagnetic interactions (typically less than a magnitude of 1 K) between neighboring molecules, as these should only be observable at much lower temperatures. Zero-field splitting of the Cr^{III} ions could also cause a low-temperature decrease in χT, but likewise, this is only expected to occur at much lower temperatures (< 30 K).

Focusing only on the $S_T = 4$ ground state that is the only thermally populated state even up to room temperature, another way to explain the decrease in χT below 150 K could be due to an unusual energy ordering of its M_S microstates. The magnetic properties of the complex could be therefore modelled considering a single $S_T = 4$ spin, with axial and transversal zero-field splitting parameters D and E introduced to implement a typical ladder of M_S microstates. Such an approach again only results in producing a low-temperature χT decrease below 30 K. Our current hypothesis is that a more sophisticated combination of crystal field parameters is necessary to describe how the energy arrangement of the M_S microstates leads to the deviation of the magnetic susceptibility from the $S_T = 4$ Curie law. However, due to the risk of overparameterization, as well as an unclear interpretation of the meaning of such parameters for a total molecular spin, this approach was not pursued.

Density functional theory (DFT) calculations. Electronic structure calculations were carried out with ORCA computational chemistry package[5] using two computational approaches: (i) with a pure functional and the double-zeta quality basis set BP86/def2-SVP and (ii) with hybrid functional and the triple-zeta quality basis set B3LYP/def2-TZVP. Approach (i) was carried out first to gain a starting point for the more computationally expensive approach (ii). Only the results of approach (ii) are reported in the main text as pure functionals like BP86 tend to overestimate spin delocalisation, leading to an overestimation of the antiferromagnetic exchange.

The exchange interaction was estimated assuming an Ising spin Hamiltonian,[6] which gives a simple closed-form expression for exchange for any spin system (this is not always possible for Heisenberg spin Hamiltonians). Therefore, the Ising Hamiltonian was chosen for simplicity, and to compare with results on other systems, which were also calculated with Ising spin Hamiltonians.

Table S1. Selected crystallographic data and parameters for **1**.

Parameter	
Formula	$C_{118.8}H_{224.3}Cr_4F_{24}N_{32.7}O_{46.7}S_8$
Formula Weight g mol^{-1}	3778.61
Crystal System	Triclinic
Space Group	$P\bar{1}$
***T*, K**	120
***a*, Å**	18.762(2)
***b*, Å**	18.9475(18)
***c*, Å**	25.561(2)
***α*, °**	107.535(5)
***β*, °**	108.776(6)
***γ*, °**	92.414(6)
***V*, Å^3**	8105.3(14)
Z	2
ρ_{calcd}, g cm^{-3}	1.345
μ (Mo Kα) mm^{-1}	0.466
R_{int}	0.0569
R_1 ($I > 2\sigma(I)$)[a]	0.1172
wR_2 (all data)[b]	0.2968
Goof on F^2	1.037

[a] $R_1 = \Sigma|(|F_o| - |F_c|)|/\Sigma|F_o|$; [b] $wR_2 = \{\Sigma[w(F_o^2 - F_c^2)^2]/\Sigma[w(F_o^2)^2]\}^{1/2}$

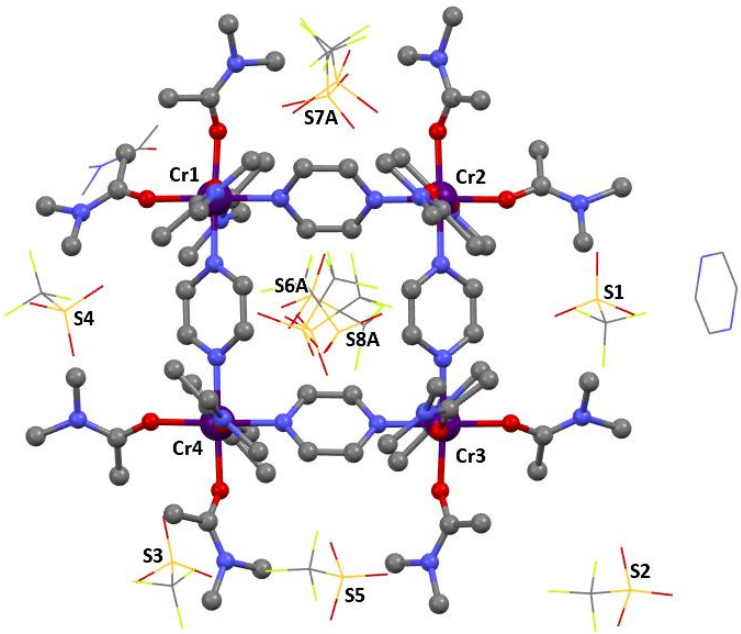

Figure S1. Molecular representation of **1** at 120 K emphasizing the chromium square cation. Only chromium ions and the S atoms of the eight $^{-}$OTf anions balancing the charge are labelled. Hydrogen atoms and uncoordinated, highly disordered solvent molecules are omitted for clarity. Color code: light blue, N; light grey, C; red, O; purple, Cr; yellow, F; orange, S.

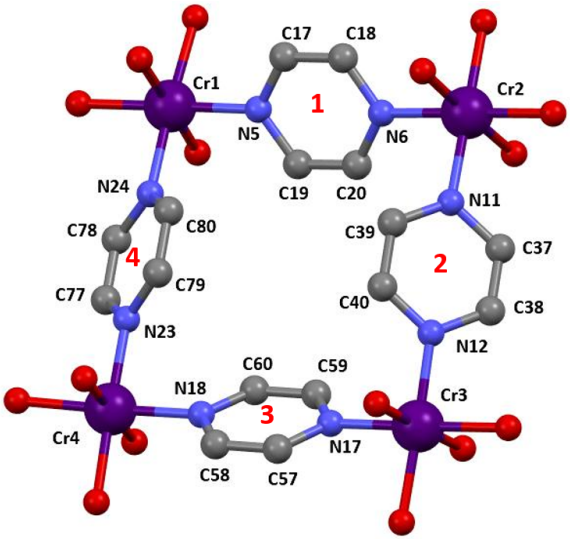

Figure S2. The molecular structure of the cationic square complex $[Cr^{III}_4(pyz^{\bullet-})_4]^{8+}$ in **1** at 120 K. The pyrazine rings are named with numbers in red to clarify the discussion of the orientations in the main text and in Table S2. Color code: light blue, N; light grey, C; red, O; purple, Cr.

Table S2. For **1**, selected bond distances, the four N-Cr-N angles, and the angles between the least-square planes defined by the atoms of each pyrazine and the chromium atoms of the square complex (Cr1 Cr2 Cr3 Cr4), at 120 K. Distances and angles are given in (Å) and (°), respectively.

Atom pair	distance (Å)	Atom pair	distance (Å)	Atom pair	distance (Å)
Cr1-N5	1.979(4)	Cr2-N6	1.974(4)	Cr3-N12	1.969(4)
Cr1-N24	1.986(5)	Cr2-N11	1.975(4)	Cr3-N17	1.964(4)
Cr1-O2	2.023(4)	Cr2-O6	2.026(4)	Cr3-O12	1.991(4)
Cr1-O4	1.995(4)	Cr2-O7	1.987(4)	Cr3-O9	2.039(4)
Cr1-O3	1.979(4)	Cr2-O5	2.034(4)	Cr3-O10	2.022(4)
Cr1-O1	2.029(4)	Cr2-O8	1.988(4)	Cr3-O11	1.998(4)
Cr4-N23	1.975(5)	N5-C17	1.362(8)	N11-C37	1.382(6)
Cr4-N18	1.978(4)	N5-C19	1.382(6)	N11-C39	1.358(7)
Cr4-O16	1.982(4)	C17-C18	1.356(8)	C38-C37	1.345(8)
Cr4-O14	2.020(4)	N6-C18	1.373(6)	N12-C38	1.368(7)
Cr4-O13	2.028(4)	N6-C20	1.364(7)	N12-C40	1.372(6)
Cr4-O15	1.976(5)	C20-C19	1.360(8)	C40-C39	1.375(8)
N17-C57	1.359(7)	N23-C77	1.387(7)	Cr1-Cr2	6.7980(15)
N17-C59	1.394(7)	N23-C79	1.346(7)	Cr2-Cr3	6.7627(16)
C58-C57	1.367(8)	C78-C77	1.347(9)	Cr3-Cr4	6.7827(15)
N18-C58	1.354(7)	N24-C78	1.347(8)	Cr1-Cr4	6.7771(17)
N18-C60	1.377(7)	N24-C80	1.395(6)	Cr1-Cr3	9.6711(17)
C60-C59	1.357(8)	C80-C79	1.364(8)	Cr2-Cr4	9.4856(17)
$\Phi_{(N5\text{-}Cr1\text{-}N24)}$	89.86(18)	$\Phi_{(pyz1\ -\ Cr\ square\ plane)}$	pyz1 (N5 C17 C18 N6 C20 C19)		39.351(2)
$\Phi_{(N6\text{-}Cr2\text{-}N11)}$	90.27(17)	$\Phi_{(pyz2\ -\ Cr\ square\ plane)}$	pyz2 (N11 C37 C38 N12 C40 C39)		38.815(1)
$\Phi_{(N12\text{-}Cr3\text{-}N17)}$	89.89(17)	$\Phi_{(pyz3\ -\ Cr\ square\ plane)}$	pyz3 (N17 C57 C58 N18 C60 C59)		40.361(2)
$\Phi_{(N18\text{-}Cr4\text{-}N23)}$	90.47(18)	$\Phi_{(pyz4\ -\ Cr\ square\ plane)}$	pyz4 (N23 C77 C78 N24 C80 C79)		40.151(1)

Table S3. Selected Cr-N_{pyz} bond distances (Å) from known single crystal structures.[7]

	$Cr^{III}Cl_2[(pyz)_2^{\bullet-}]$	$Cr^{III}Br_2[(pyz)_2^{\bullet-}]$		$Cr^{III}(NCS)_2[(pyz)_2^{\bullet-}]$	$Cr^{II}I_2(pyz)_2$
T **/K**	120	120	300	300	120
Cr-N2$_{pyz}$ /Å	2.018(3)	2.081(4)	2.079(5)	2.054(4)	2.149(4)
Cr-N1$_{pyz}$ /Å	2.071(3)	2.024(4)	2.040(4)	2.054(4)	2.149(4)

Table S4. Bond valence sum (BVS) calculations.[8]

Atom	Cr1	Cr2	Cr3	Cr4
Calculated as Cr(II)	+3.21	+3.23	+3.23	+3.26
Calculated as Cr(III)	+2.95	+2.96	+2.97	+2.99

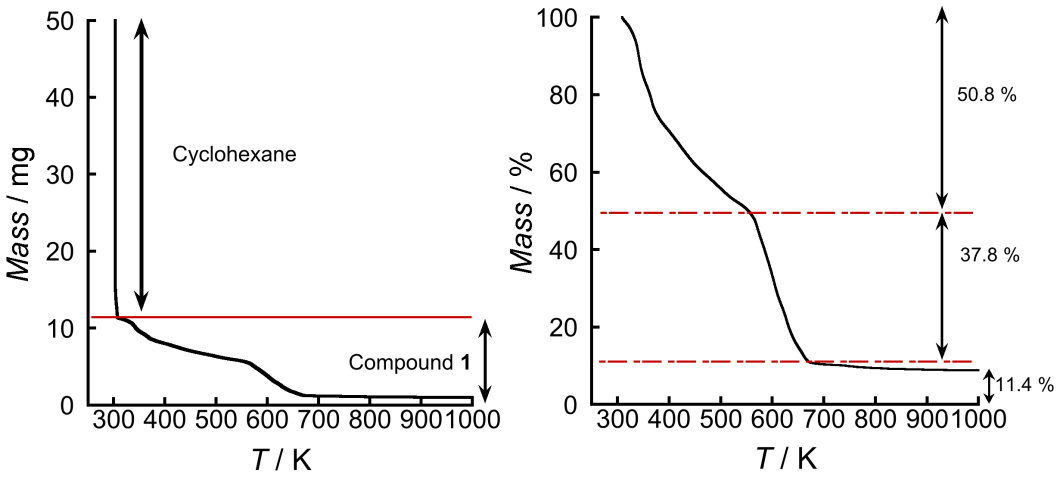

Figure S3. Left: Thermogravimetric analysis (TGA) of **1** under a flow of nitrogen at a heating rate of 2 K min^{-1}. Right: TGA plot calculated from the original data shown in the left part of the figure after subtracting the mass corresponding to protecting cyclohexane (*vide supra*). The initial mass drop in the left plot corresponds to the evaporation of cyclohexane (38.85 mg) at 310 K under the N_2 flow in the furnace before the start of the heating. Right plot: expected weight loss percentages for **1**: 1 DMA, 2.3 %; 22.7 DMA, 52.3 %; 1 OTf, 3.9 %; 8 OTf, 31.6 %; 1 pyz, 2.1 %; 5 pyz, 10.6 %; 4 CrF_3, 11.4 %, 12 F, 6.0 %. The results indicate that (a) the 1st step (310-560 K, 50.8 %) is consistent with the continuous loss of the DMA molecules and the interstitial pyrazine (22.7 DMA and one pyrazine molecules, calc: 54.4 %), (b) the 2nd step (560-675 K, 37.8 %) likely corresponds to the further decomposition of the four pyrazine ligands of the square complex and the 8 $^{-}$OTf anions, with a release of 12 F atoms, which react with Cr centers during the process (calc: 34.1 %), (c) the residual weight percentage for the 3rd step (675-1000 K, 11.4 %) is in agreement with the weight expected for 4 CrF_3 (calc: 11.4 %).[9]

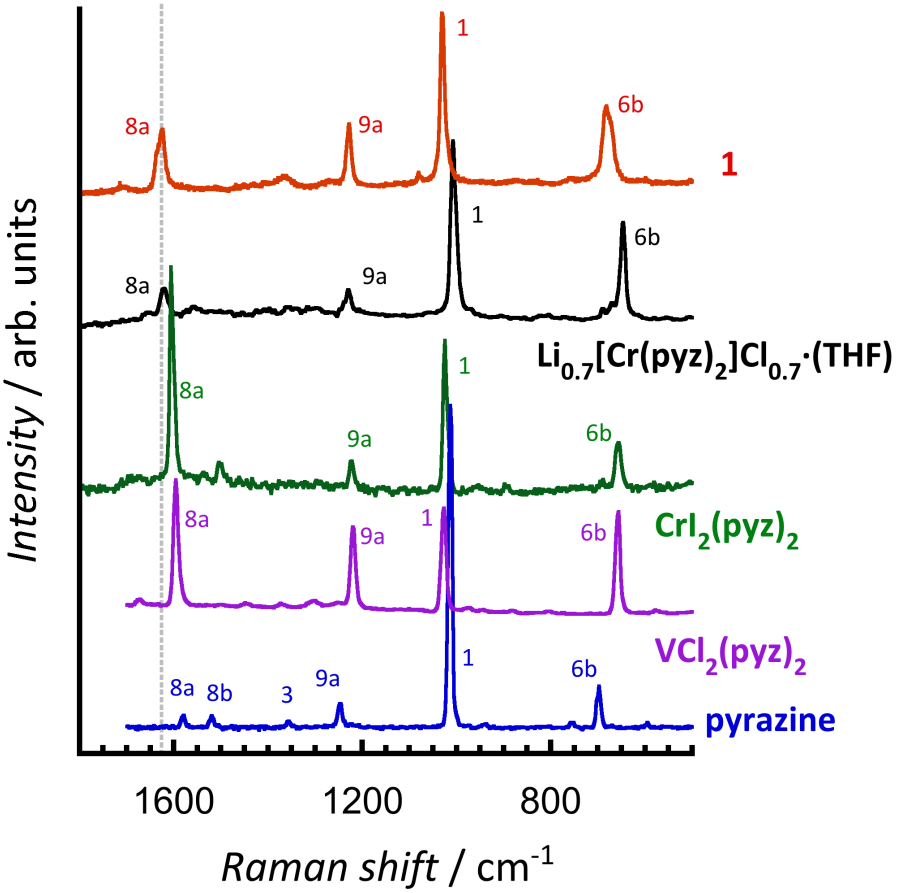

Figure S4. Raman spectroscopy (λ = 785 nm) of neutral pyrazine (blue trace), $VCl_2(pyz)_2$ (purple trace), $CrI_2(pyz)_2$ (green trace), $Li_{0.7}[Cr(pyz)_2]Cl_{0.7}\cdot(THF)$ (black trace), and **1** (red trace) between 1800 and 500 cm^{-1} recorded at room temperature. The labelling denotes the Wilson nomenclature:[10] **8a**: *sym*. C=C stretching and C-H scissoring; **8b**: *asym*. C-N stretching; **3**: C-H rocking; **9a**: C-H scissoring; **1**: C-H scissoring, in-plane ring-breathing; **6b**: asym. in-plane ring-deformation. Peak assignment for pyrazine: 1578 cm^{-1} – **8a**; 1518 cm^{-1} – **8b**; 1356 cm^{-1} – **3**; 1246 cm^{-1} – **9a**; 1013 cm^{-1} – **1**; 700 cm^{-1} – **6b**. Peak assignment for $VCl_2(pyz)_2$: 1598 cm^{-1} – **8a**; 1221 cm^{-1} – **9a**; 1027 cm^{-1} – **1**; 654 cm^{-1} – **6b**. Peak assignment for $CrI_2(pyz)_2$: 1605 cm^{-1} – **8a**; 1221 cm^{-1} – **9a**; 1027 cm^{-1} – **1**; 658 cm^{-1} – **6b**. Peak assignment for $Li_{0.7}[Cr(pyz)_2]Cl_{0.7}\cdot(THF)$: 1620 cm^{-1} – **8a**; 1229 cm^{-1} – **9a**; 1007 cm^{-1} – **1**; 646 cm^{-1} –**6b**.[11] Tentative peak assignment for **1**: 1625 cm^{-1} – **8a**; 1225 cm^{-1} – **9a**; 1031 cm^{-1} – **1**; 682 cm^{-1} – **6b**.

Among the four major peaks in the spectra of pyrazine-bridged systems, the **8a** mode, which involves C=C stretching and C-H scissoring,[11] has been determined as the most appropriate marker to investigate the effect of pyrazine reduction. Metal-organic systems with reduced pyrazine bridges tend to have the band **8a** in the 1620–1625 cm^{-1} frequency range whereas systems with neutral pyrazine bridges tend to have band **8a** in the 1598–1605 cm^{-1} range. The

studied complex falls in the range of systems with reduced pyrazine, supporting the hypothesis of Cr^{III} with fully reduced pyrazine ligands.

While it is true that steric effects also play a role in the shift of **8a**, due to the influence of C-H scissoring in the mode,[11] we argue that among the four bands, **8a** should be the band *most* sensitive to the pyrazine oxidation state. This is because the force constant of C=C stretching vibrations, and thus the related energy, is directly affected by pyrazine reduction. In contrast, the energies of pyrazine ring deformations (**1** and **6b**) are affected by steric interactions between the pyrazine ring and its environment, which depend on the whole crystal/molecular structure. Finally, the **9a** C-H scissoring mode is not expected to be significantly affected by the reduction of pyrazine, and experimental data corroborate this statement since the energies of the corresponding Raman band for the four coordinated compounds are all in the 1220–1230 cm^{-1} range.

Table S5. Estimated exchange coupling constant *J* between Cr^{III} and radical pyrazine spins, and the Mulliken spin population on Cr site in its high-spin state (and in broken-symmetry state).

Method	*J*, cm^{-1} (in K)	Spin population on the Cr site
B3LYP/def2-TZVP	-648 (-932)	3.1 (3.0)
BP86/def2-SVP	-947 (-1363)	3.1 (2.7)

The effective spin-Hamiltonian assumes 4-fold symmetry and identical exchange coupling between chromium(III) spins and neighboring pyrazine radical spins neglecting all other exchange coupling interactions:

$$\widehat{H} = -2J\left(\hat{S}_{1z}^{Cr}\hat{S}_{1z}^{R} + \hat{S}_{2z}^{Cr}\hat{S}_{1z}^{R} + \hat{S}_{2z}^{Cr}\hat{S}_{2z}^{R} + \hat{S}_{3z}^{Cr}\hat{S}_{2z}^{R} + \hat{S}_{3z}^{Cr}\hat{S}_{3z}^{R} + \hat{S}_{4z}^{Cr}\hat{S}_{3z}^{R} + \hat{S}_{4z}^{Cr}\hat{S}_{4z}^{R} + \hat{S}_{1z}^{Cr}\hat{S}_{4z}^{R}\right)$$

In the high-spin state, Cr(III) site has spin projection $M_{S^{Cr}} = \pm 3/2$ and each pyrazine radical has the spin projection $M_{S^{R}} = \pm 1/2$, the energy of the high-spin state is $E^{HS} = -12J$. The broken-symmetry solution where all Cr sites have positive spin projection $M_{S^{Cr}} = 3/2$ and pyrazine radicals have negative spin projection $M_{S^{R}} = -1/2$ has an energy of $E^{BS} = 12J$. Hence, the exchange coupling could be estimated as:

$$J = -\frac{E^{HS} - E^{BS}}{24}$$

References

1. P. Perlepe, I. Oyarzabal, K. S. Pedersen, P. Negrier, D. Mondieig, M. Rouzières, E. A. Hillard, F. Wilhelm, A. Rogalev, E. A. Suturina, C. Mathonière and R. Clérac, *Polyhedron*, 2018, **153**, 248–253.

2. E. Coronado, *Nat. Rev. Mater.*, 2019, **5**, 87–104.

3. G. M. Sheldrick, *Acta Crystallogr. Sect. C Struct. Chem.*, 2015, **71**, 3–8.

4. A. L. Spek, *Acta Crystallogr. Sect. C Struct. Chem.*, 2015, **71**, 9–18.

5. F. Neese, *WIREs Comput. Mol. Sci.*, 2012, **2**, 73–78.

6. D. Dai and M.-H. Whangbo, *J. Chem. Phys.*, 2003, **118**, 29–39.

7. L. Voigt, PhD thesis, Technical University of Denmark, 2020.

8. I. D. Brown and D. Altermatt, *Acta Crystallogr. Sect. B*, 1985, **41**, 244–247.

9. W. E. Buschmann and J. S. Miller, *Chem. Eur. J.*, 1998, **4**, 1731–1737.

10. E. B. Wilson, *Phys Rev.*, 1934, **45**, 706-714.

11. P. Perlepe, I. Oyarzabal, A. Mailman, M. Yquel, M. Platunov, I. Dovgaliuk, M. Rouzières, P. Négrier, D. Mondieig, E. A. Suturina, M.-A. Dourges, S. Bonhommeau, R. A. Musgrave, K. S. Pedersen, D. Chernyshov, F. Wilhelm, A. Rogalev, C. Mathonière and R. Clérac, *Science*, 2020, **370**, 587–592.